University of Baghdad
College of Engineering
JOURNAL OF ENGINEERING

Journal of Engineering
journal homepage: www.jcoeng.edu.iq
Volume 31 Number 5 May 2025

The Effect of Non-Thermal Plasma on the Structural and Optical Characteristics of SnO_2:Co Thin Films Prepared by Spray Pyrolysis Technique

Randa Mohammed *, **Ramiz Ahmed Al- Ansari**

Department of Physics, College of Science for Women, University of Baghdad, Baghdad, Iraq

ABSTRACT

This study used a spray pyrolysis approach to create thin films from SnO_2 doped with 2% Co on a heated glass substrate at 400°C and investigated how the structural and optical characteristics are affected by non-thermal plasma. X-ray diffraction analysis was initially employed to look into the structural characteristics, and the results indicate that the SnO_2 and SnO_2:Co thin film are polycrystalline and have tetragonal structure, peak formation has occurred in (110), (101), and (211), which correlate to the subsequent diffraction angles, respectively (26.55^0), (33.90^0), and (51.55^0). A peak associated with Co was also observed at (311), which is equivalent to the (36.78^0) diffraction angle. According to AFM analysis, the grain size decreases from 64.01 nm to 59.10 nm after doping. Roughness and root mean square also appears to increase after doping, according to the UV-VIS spectrometer analysis, the transmittance increases with doping and decreases with non-thermal plasma exposure, the energy gap value increases during Non-thermal plasma exposure and its decrease after doping. Additionally, the absorbance, absorbance coefficient, refractive index and extinction coefficient rise following Cold plasma exposure.

Keywords: SnO_2:Co, Spray pyrolysis, Non-thermal plasma, Structure properties, Optical properties.

1. INTRODUCTION

Beyond the well-known solid, liquid, and gas states, plasma is recognized as the fourth state of matter. There are two primary categories of plasma based on temperature: low-temperature and high-temperature plasma, also known as gas discharges, are present in a high-temperature plasma where all of its particle species—including electrons, ions, and neutral particles are in thermal equilibrium ($T_e \approx T_i \approx T_n$). Additionally, low temperature plasma is separated into two sub-sections: The components of thermal plasma are in a condition of local equilibrium, while the

*Corresponding author
Peer review under the responsibility of University of Baghdad.
https://doi.org/10.31026/j.eng.2025.05.11

Article received: 08/10/2024
Article revised: 01/02/2025
Article accepted: 04/02/2025
Article published: 01/05/2025

electrons in non-thermal plasma, also known as cold plasma, has a temperature that is significantly greater than that of the other components: ($T_e \gg T_i \approx T_n$). **(Abdalameer, 2017).** Dielectric barrier discharge (DBD), with its huge volume plasma feature, provides one of the most efficient non-thermal plasma sources at atmospheric pressure. Additionally, because the equipment is simple to use, requires no costly vacuum system, and has cheap operating and maintenance costs. **(Abdullah et al., 2012; Brandenburg, 2017).** The SnO2: Co thin films were subjected to non-thermal plasma (FE-DBS), which is composed of a 150 mm copper cylinder with a 2 mm spindle diameter, the spindle's opposite end is attached to a High Voltage (HV) connector and its ends are connected to a floating base with a 20 mm diameter.(SnO_2) thin films are one of the semiconducting oxide nanostructures, It is receiving a lot of attention due to their Chemical and Physical characteristics, It is well known that n-type semiconductors **(Mazloom, 2013; Bendjedidi et al., 2015)** have a wide range of uses and have a large band gap of 3.6–3.8 eV **(Saadeddin et al., 2007; Mohammed, 2012),** including as transparent conducting electrodes, heat reflectors in solar cells, different gas sensors **(Abdullah et al., 2012; Bahade et al., 2017; Chen et al., 2024)**. Numerous benefits of thin film technology for the photovoltaic industry include cheap cost, minimal material and energy usage, and ease of access. It has the highest sensitivity and selectivity behavior, making it one of the best options for gas sensor applications, strong chemical bonds, great oxidizing power, non-toxicity, and special transport qualities **(Gupta and Rathore, 2020)**. Numerous methods have been employed to deposit tin oxide (SnO_2) thin films, among them RF-Sputtering **(Enoki et al., 1992; Ma et al., 2005)**. sol-gel **(Guendouz, et al., 2018; Labreche et al., 2018).** Chemical vapor deposition **(Shi et al., 2010; Yang et al., 2014)**. and spray pyrolysis **(Serin et al., 2006; Benhaoua et al., 2015; Abdelkrim et al., 2016).** Spray pyrolysis is one of these methods that has been shown to be easy to use, affordable, and repeatable **(Sawant et al., 2021; Vossen and Poliniak, 1972)**. This research aims to manufacture thin films of SnO_2 material doped with 2% Co by using the spray pyrolysis technique (SPT) on the glass substrate heated to 400 ^{0} C, after exposure to non-thermal plasma for different exposure times (3,5,7 sec), and study the structure and optical properties

2. EXPERIMENTAL WORK

Using the chemical spray pyrolysis method, pure and doped Co in SnO_2 thin films were created. A solution of tin chloride salts ($SnCl_4.5H_2O$)(Loba Chemie, India) was used to create tin oxides, a white solid with a molecular weight of 350.58 g/mole, which was made in 0.1 M, In 100 ml of pure water **(Enoki et al., 1992; Dangi et al., 2023),** the (3.5058) g of tin chloride was dissolved. In order to guarantee the total dissolving of the material, a magnetic stirrer was used to agitate this mixture for 30 minutes, yielding a uniformly white solution. Glass bases were cleaned and allowed to dry. Additionally, they measured (2.5×2.5) cm, Afterwards, the mixture was sprayed onto glass bases that had been heated to 400°C. A tin oxide layer was placed on the base using the spray pyrolysis method, using cobaltous chloride ($CoCl_2.6H_2O$) as a source of cobalt oxide to create the solution. Cobalt oxide is a solid with a pink hue and a molecular weight of 237.93 g/mole, was added to the prior tin oxide solution, and the mixture was then magnetically stirred for (30 minutes) to produce a well-homogenous mixture, after that, the glass was heated to 400^{0}C and then the solution was sprayed on it. The doped sample was then exposed to the non-thermal plasma for 3, 5, and 7 seconds.

3. RESULTS AND DISCUSSION

3.1 (X-ray) Diffraction

The thin films of SnO_2 and SnO_2: Co were created by the spray pyrolysis technique are shown in **Fig. 1** and **Fig. 2** the polycrystalline structure of tetragonal rutile structure was shown by (XRD) analysis of both the pure SnO_2 film and SnO_2: Co **(Bendjedidi et al., 2015; Paneru, 2019; Soumya and Xavier, 2022)**. For the pure samples, The peaks to SnO_2 correspond to (110),(101),(111),(211),(002),(301),and(321)when2θ(26.55^0),(33.82^0),(38.93^0),(51.70^0), (57.7^0), respectively. Bragg reflections are observed with peaks of (110), (211) at 2θ =(26.55^0),(51.55^0), the peak of 2 % Co corresponds to (111) when 2θ= (45.91^0) Because of the self-composition phenomena, reflectance values show a strong degree of crystallinity, with a noticeable crest that is mostly found in the directionality of (110), **Table 1,** show all Structural parameters .

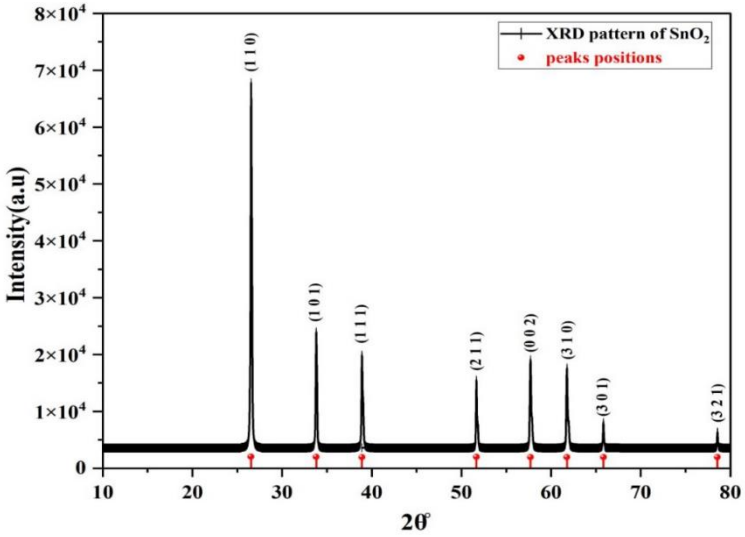

Figure 1. the XRD for a SnO_2 thin film made using the spray pyrolysis

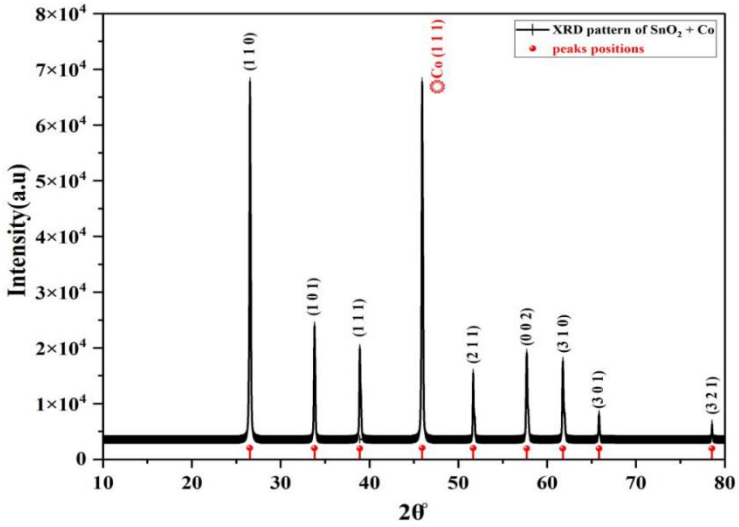

Figure 2. The XRD of SnO_2: Co thin film made using the spray pyrolysis method

Table 1. Structure parameters for pure SnO_2 and SnO_2: Co thin films prepared by spray pyrolysis

Sample	2θ°	FWHM (°)	d_{hkl} Exp.(A°)	G.s(nm)	Av. G. s	d_{hkl} Std.(A°)	Phase	hkl	Card No.
SnO_2	26.556	0.188	3.357	43.189	39.264	3.355	Tetragonal	110	01-077-0450
	33.826	0.221	2.649	37.525		2.649	Tetragonal	101	01-077-0450
	38.935	0.213	2.313	39.399		2.313	Tetragonal	111	01-077-0450
	51.705	0.230	1.767	38.266		1.767	Tetragonal	211	01-077-0450
	57.727	0.268	1.596	33.751		1.596	Tetragonal	002	01-077-0450
	61.796	0.279	1.501	33.132		1.500	Tetragonal	310	01-077-0450
	65.854	0.228	1.417	41.408		1.417	Tetragonal	301	01-077-0450
	78.563	0.216	1.217	47.444		1.216	Tetragonal	321	01-077-0450
SnO_2 : Co	26.556	0.175	2.352	46.454	42.674	3.355	Tetragonal	110	01-077-0450
	33.826	0.232	1.675	35.741		2.649	Tetragonal	101	01-077-0450
	38.935	0.245	3.344	34.328		2.313	Tetragonal	111	01-077-0450
	51.705	0.233	2.023	37.728		1.767	Tetragonal	211	01-077-0450
	45.912	0.1323	1.978	67.643		1.974	Cubic	111	01-088-2325
	57.727	0.245	1.543	36.946		1.500	Tetragonal	310	01-077-0450
	61.796	0.232	1.557	39.821		1.417	Tetragonal	301	01-077-0450
	65.854	0.255	1.321	37.039		1.216	Tetragonal	321	01-077-0450
	78.563	0.212	1.417	48.365		1.332	Tetragonal	110	01-077-0450

The study shown that deformation with Co caused the granular size to rise, indicating enhanced crystallization in line with research findings **(Mohsin et al., 2022; AL-Jawad et al., 2016)** Full width at half maximum (FWHM) shows that the width of the curve decreases in the center of the apex after doping by Co deformation, indicating a rise in grain size since, as Scherer's Equation shows.

3.2 Atomic Force Microscope (AFM)

It was employed to investigate the topology of the (SnO_2) film's surface as well as the impact of (Co) Deformation., The pure sample has both nanostructured and uniformly distributed, with an average diameter of approximately 64.01 nm, RMS roughness of approximately 31.26 nm, and roughness of 24.37 nm, according to the results of the AFM investigation. After doping, the grains decrease in size which is equal to (59.10 nm) and the roughness and (RMS) increase after doping, equal to (31.41nm) and (41.08 nm) respectively, which causes the reactivity of gases to the sensor surface to grow.

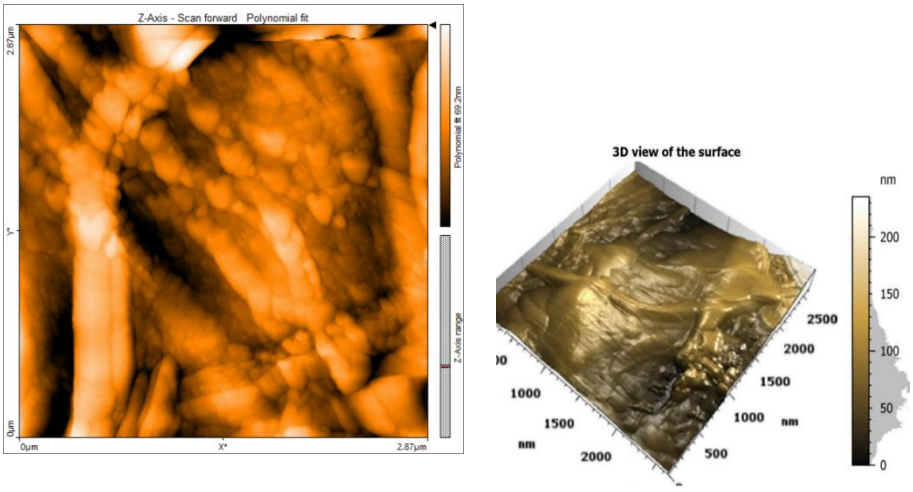

Figure 3. The AFM for SnO_2 Thin Films

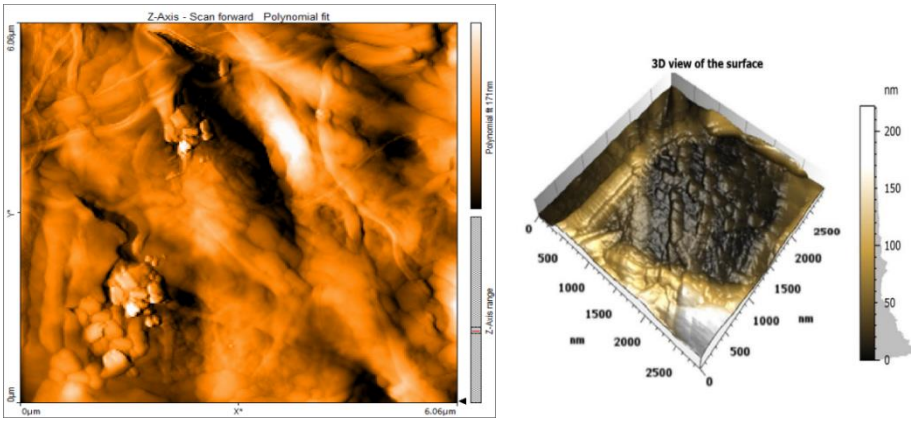

Figure 4. The AFM of a thin sheet of SnO_2: Co Thin Films

3.3 The Measurement of Thin Film Thickness

3.3.1 AFM Thickness Measurement

Since it affects the film's physical properties, thickness is an important consideration. There are two ways to determine the film's thickness, there are distinct ways to measure the specimen cross section: AFM and TEM, **(Bhatt et al., 2020).**

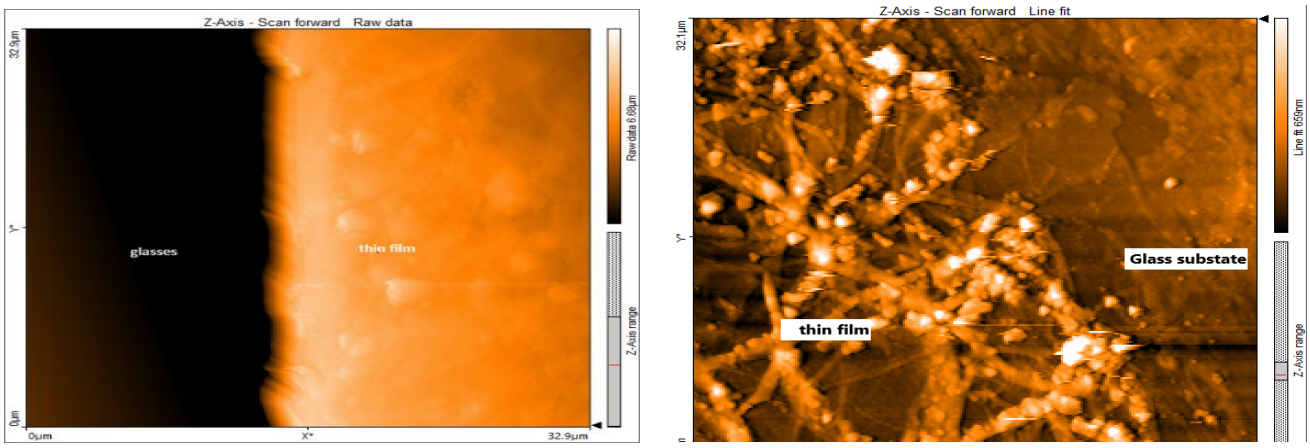

(A) **(B)**

Figure 5. AFM thickness measurement of (A)SnO_2 and (B)SnO_2: Co thin film

3.3.2 Optical Method

The thickness of SnO_2: Co and pure SnO_2 was calculated using the following formula and the interference photic method with He-Ne at a wavelength of 632.8 nm and an angle of 450.

$$t = \frac{\Delta x}{x} \frac{\lambda}{2} \quad (1)$$

The values of X and t represent the dazzling fringe width and thickness, respectively, in nanometers. ΔX is the opaque fringe width in nanometers. λ is the incident laser beam's wavelength in nanometers. The thicknesses of SnO_2 and SnO_2: Co thin films, measured using AFM and optical methods were equal to 127.2 and 142.15 nm, respectively.

3.4 OPTICAL PROPERTIES

3.4.1Transmittance

It was found that the transmittance of the thin films made from pure SnO_2 is equivalent to 77.80 % in the visible field. **Fig. 6** shows the impact of wavelength on the transmittance in the 300-900 nm region for both pure and doped 2 % SnO_2:CO While the transmittance of the doped thin film SnO_2:Co reduces to 64.70% in the visible spectrum and near-infrared region, this decrease in transmittance occurs after doping due to the deformation of the cobalt particles, which causes the tin oxide particles to fill in these spaces between them, and also because the thickness increase after doping this lead to reduce the transmittance, this result identical with the research **(Bouabdalli et al., 2021).** The transmittance spectrum is affected by non-thermal plasma, as seen in **Fig. 8** where the transmittance of the film decreases with longer exposure times to non-thermal plasma, particularly at time (7 sec).

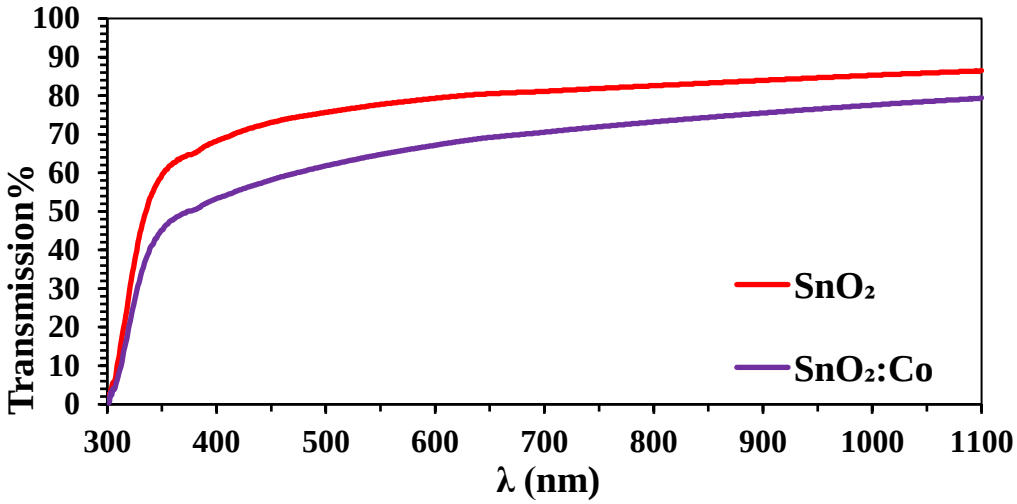

Figure 6. Illustration of the transmission of SnO_2 and SnO_2: Co thin films.

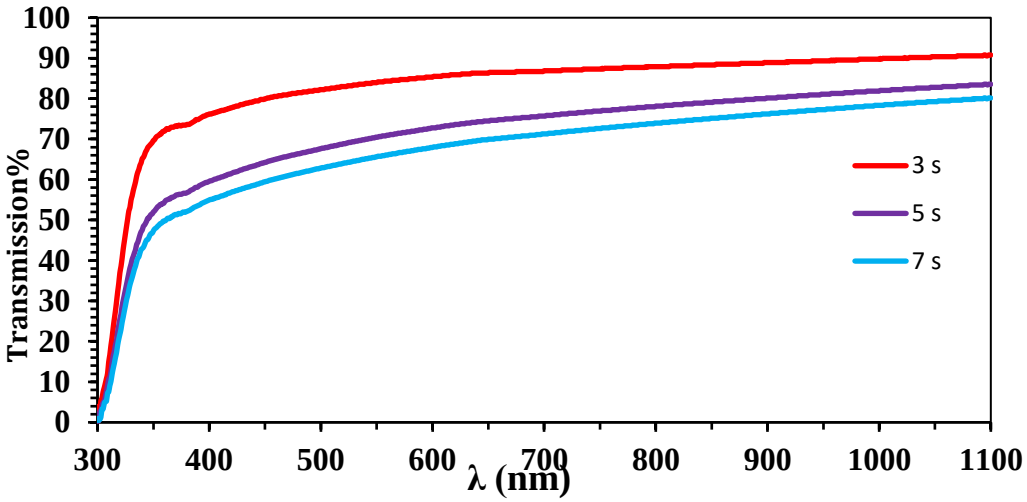

Figure 7. The non-thermal plasma effects on SnO_2: Co thin films at (3,5,7 sec)

4.3.2 Absorbance

Many elements, including the kind of material, thickness, and incident beam wavelength, have an impact on absorbance materials, **Fig. 8** illustrates how absorbance changes with wavelength for all substances under study within the range of 300-900 nm, Because the energy gap will narrow with increased doping, it was discovered that the absorbance increased following doping. Additionally, it was discovered that the absorbance decreased with increasing wavelength for all manufactured thin films. **Fig. 9** shows the effect of non-thermal plasma on the absorbance and it was found the absorbance increases with an increases in the exposure time of plasma, this is due to the inverse relationship between absorbance and transmittance, where transmittance and absorbance are related to the following relationship.

$$T = e^{-2.303\,A} \quad (2)$$

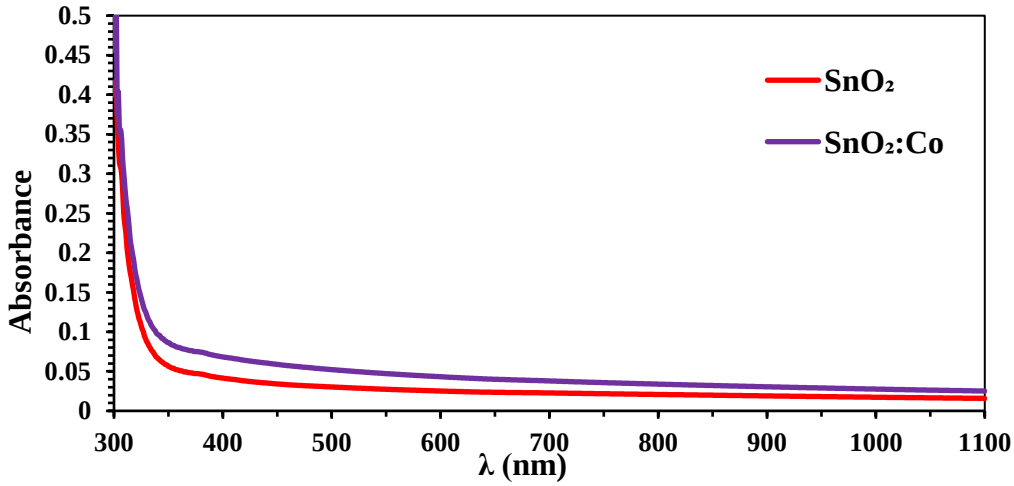

Figure 8. the absorbance for SnO_2 and SnO_2: Co thin films as a function of wavelength

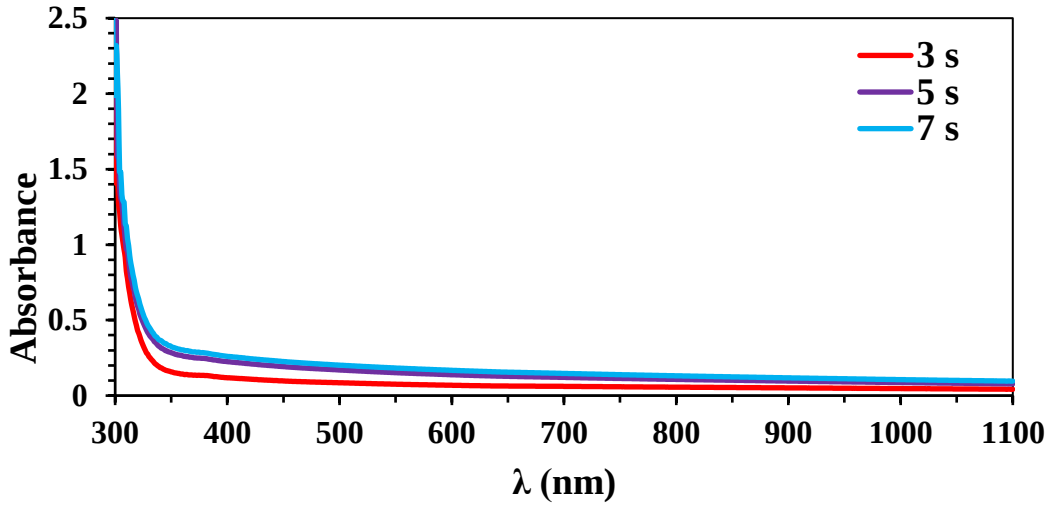

Figure 9. illustrates how non-thermal plasma effects on SnO_2: Co thin films absorbance

3.4.3 Absorption Coefficient

The absorption coefficient was computed by.

$$\alpha = \frac{2.303 \times A}{t} \quad (3)$$

where thickness is represented by t and absorbance by A. It was observed that Co-doping causes the absorption constant to increase. The absorption coefficient also shows behaviour that is opposite to the transmittance pattern; **Fig. 10** illustrates how short wavelengths cause the absorption coefficient to rise to a greater value before drastically declining with increasing wavelength. After being exposed to non-thermal plasma for (3, 5, 7) seconds, the absorption coefficient of SnO_2: Co films was calculated as a function of wavelength, as shown in **Fig. 11** It was observed that the absorption coefficient increased with longer exposure times.

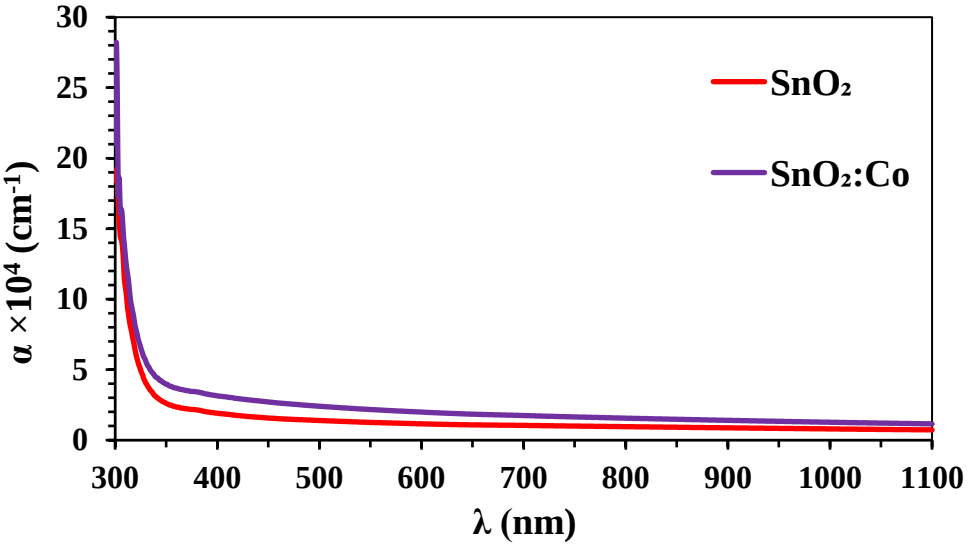

Figure 10. the SnO_2 and SnO_2: Co thin films absorption coefficients as a function of wavelength

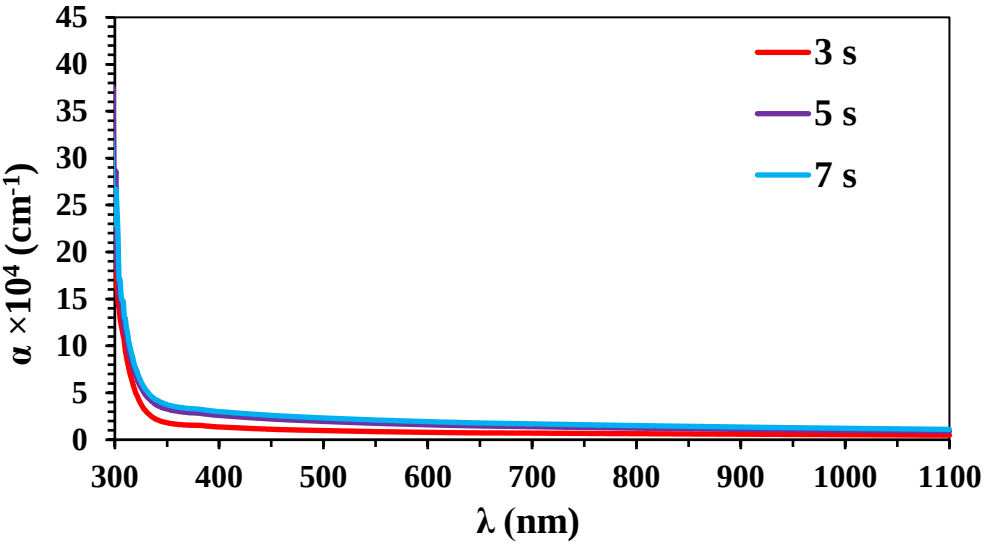

Figure 11. the effect of non-thermal plasma on the absorption coefficient of SnO_2: Co thin films

3.4.4 Optical Band Gap (E_g)

This is the absorption coefficient based on Tauc's relation **(Doyan et al., 2021)**

$$\alpha h\upsilon = B(h\upsilon - Eg)^m \quad (4)$$

in which the photon energy is represented by hυ, the energy gap by Eg, and the constant m, for direct allowed transmission for semiconductors, has a value of 1/2. In relation to the transitions, B is value fluctuates and remains constant, Graphing $(\alpha h\upsilon)^2$ versus photon

energy hυ yields the intersection point, which represents the energy gap, when the straight component of the resulting curve is stretched to cut the hυ axis at point $(\alpha h\upsilon)^2 = 0$ **(Bu et al., 2023)**. Doping influence on the energy gap, as demonstrated by **Fig .12** shows that doping changes the energy gap from (3.95 to 3.90) The formation of Charge Transfer Complexes (CTCs) in the host lattice with the introduction of modest amounts of dopants may explain the decrease in optical band gap and activation energy observed upon doping. The effect of non-thermal plasma on the energy gap is depicted in **Fig. 13** where it was found that the energy gap increases with the duration of the non-thermal plasma's exposure. Where are the energy gap values after exposure for (3, 5, 7) sec similar to (4.10, 4.05, 400 ev) correspondingly, especially on 3 sec exposure time.

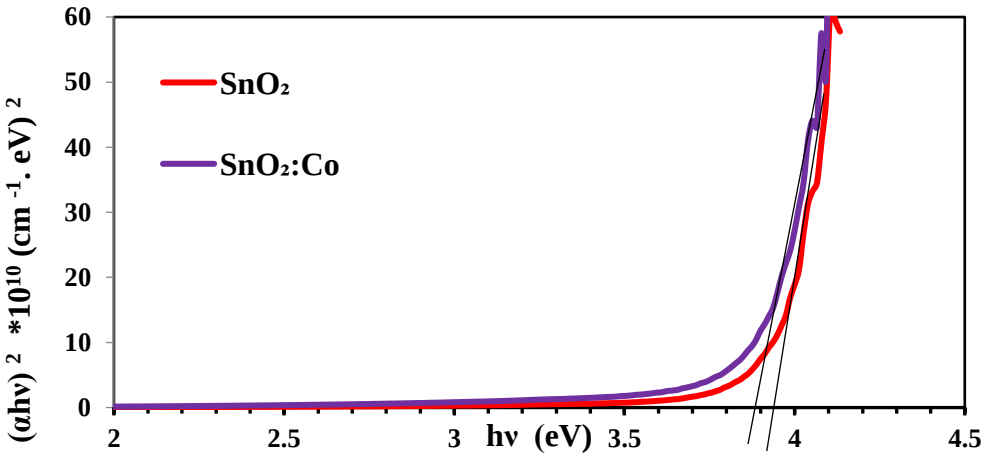

Figure 12. the energy gap of SnO_2 and SO_2: Co thin film

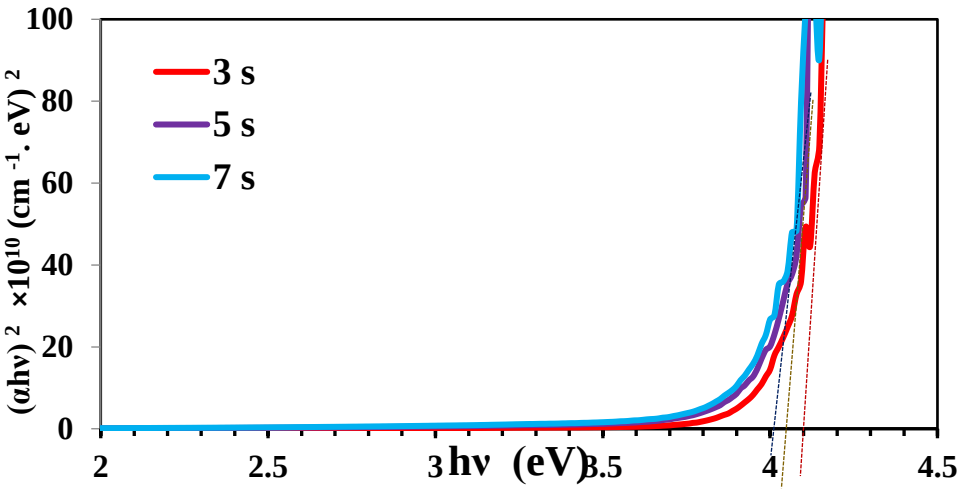

Figure 13. the effect of non-thermal plasma on the energy band gap

3.4.5 Extinction Coefficient

The extinction coefficient could be calculated by using the following equation:

$$K_o = \frac{\alpha\lambda}{4\pi} \quad (5)$$

Fig. 14 shows the extinction coefficient decreases with increase in the wavelength for all pure and doped thin film and also the figure shows the extinction coefficient increases after doping This conduct is explained by, the increase of carrier density behavior confirming the increase in the absorption coefficient. the plasma causes the extinction coefficient to rise as exposure time increases. As a result, doping with cobalt increases the extinction coefficient. The effect of non-thermal plasma on the extinction coefficient is depicted in **Fig. 15,** where longer exposure times cause the plasma to increase the extinction coefficient

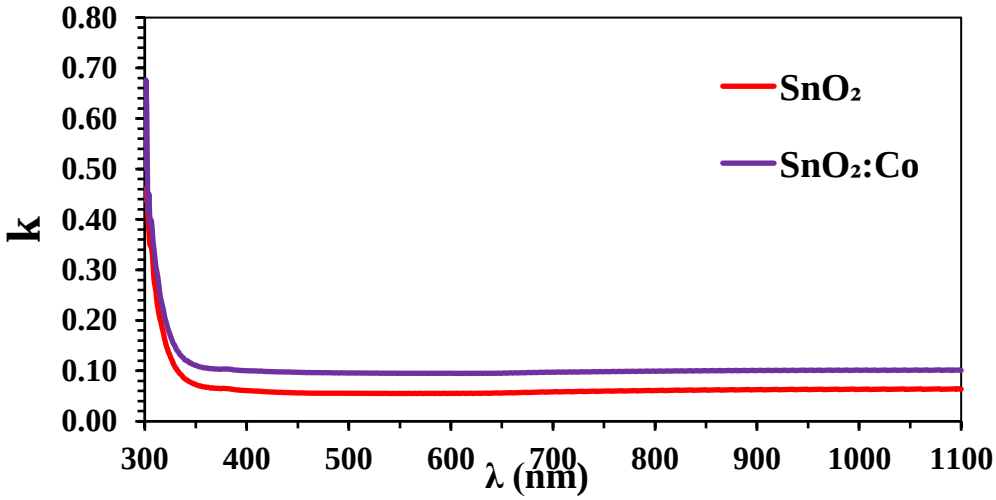

Figure 14. the SnO_2 and SnO_2: Co thin films Extinction coefficient as a function of wavelength

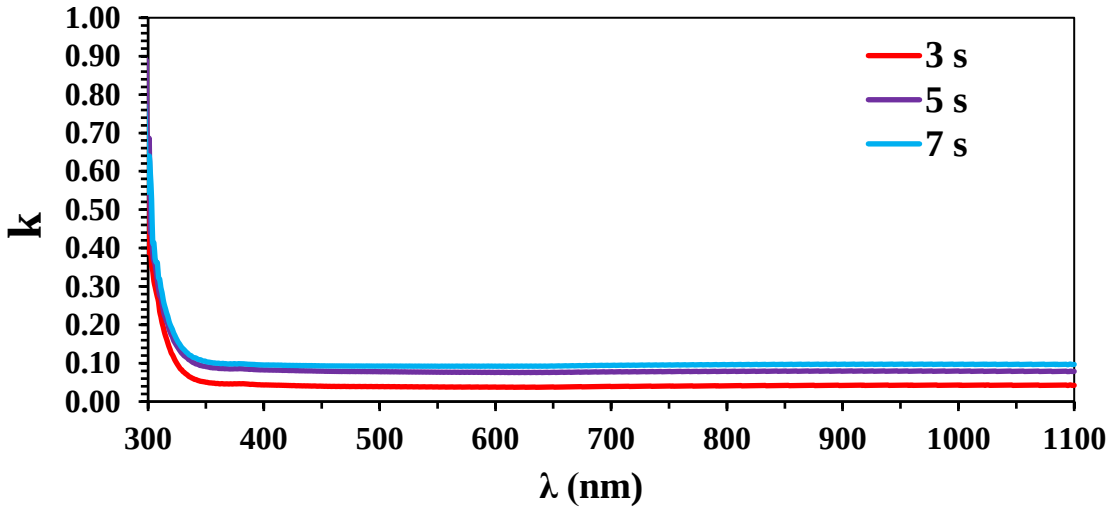

Figure 15. effect of non-thermal plasma on the SnO_2: Co thin-film extinguishing coefficient.

3.4.6 Refractive Index (n)

Fig. 16 shows the relation between the reflective index and wavelength, the reflective index increase with a decrease, wavelength which means an increase with increased energy the behavior of the reflective index is the same with reflection, also that the reflective index increases after doping 2% Co from (2.580) to (3.475), **Fig. 17** show the effect of non-thermal plasma on the reflective index, we observed the reflective index increase with an increased exposure time of plasma (3, 5, 7) which is equal to (3.115), (4.549), (5.016) respectively. The reflective index and reflection increase after doping and exposure to plasma specifically in 7 sec, where the reflective index increased from (2.580 to 5.015) after doping and exposure to 7 sec of plasma.

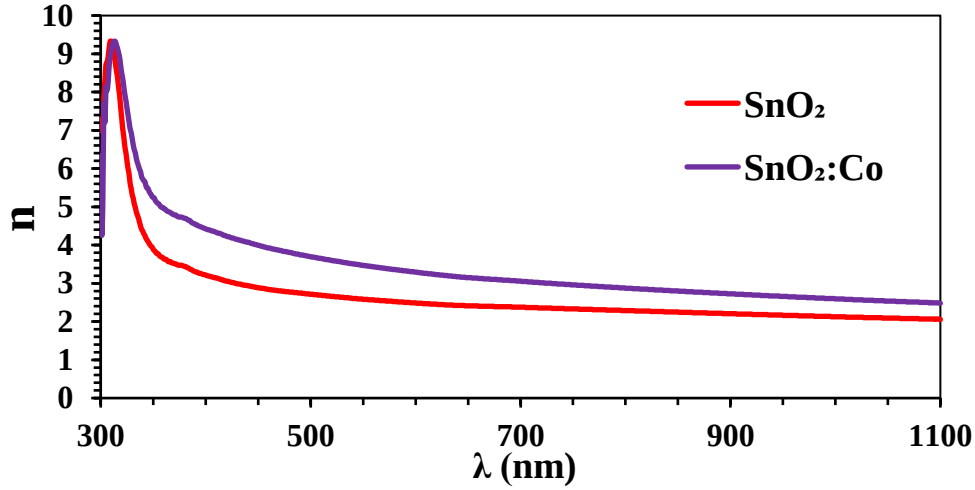

Figure 16 displays SnO_2 and SnO_2: Co reflective index as a function of wavelength

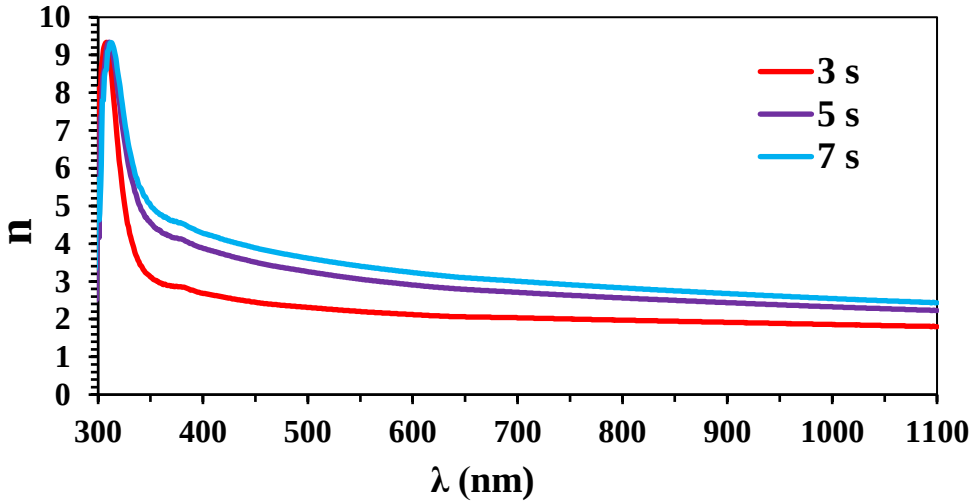

Figure 17. the effect of non-thermal plasma on the refractive in (3, 5, 7sec) of SnO_2: Co thin films

Table 3. the parameter of SnO_2 and SnO_2: Co thin film

Sample	A	α (cm^{-1})	K	n	ε_r	ε_i	Eg (eV)
SnO_2	0.11	12551	0.055	2.580	6.652	0.284	3.95
SnO_2:Co	0.19	21763	0.095	3.473	12.052	0.662	3.90

Table 4. The effect of non-thermal plasma for (3, 5, 7) sec

Time (s)	A	α (cm^{-1})	K	n	ε_r	ε_i	Eg (eV)
3	0.16	18079	0.050	3.115	9.701	0.314	4.10
5	0.28	32703	0.091	4.549	20.686	0.829	4.05
7	0.33	37424	0.104	5.016	25.154	1.046	4.00

4. CONCLUSIONS

The Thin-film manufactured from SnO_2 and SnO_2: Co by using spray pyrolysis technique showed that they belong to a tetragonal-shaped polycrystalline. also, the AFM shows the roughness and root mean square increase after doping. The transmittance decreases when exposed to non-thermal plasma, as seen in the UV, and the optical energy gap increases after exposure to non-thermal plasma, also the absorption, absorption coefficient, refractive index and extinction coefficient increase with increased plasma exposure time.

Acknowledgements

The researchers extend their thanks to the University of Baghdad, College of Science for their support of this research work.

Credit Authorship Contribution Statement

Randa Mohammed writing, editing and interpreting the results, Ramiz Ahmed Al_Ansari linguistic correction and scientific correction and reference review.

Declaration of Competing Interest

The authors declare that they have no known competing financial interests or personal relationships that could have appeared to influence the work reported in this paper.

REFERENCES

Abdalameer, N.K., 2017. Effects of cold atmospheric plasma on the optical properties of SnO_2 thin film. *Advances in Natural and Applied Sciences*, 11(9), pp.357-364.

Abdelkrim, A., Rahmane, S., Abdelouahab, O., Abdelmalek, N. and Brahim, G., 2016. Effect of solution concentration on the structural, optical and electrical properties of SnO_2 thin films prepared by spray pyrolysis. *Optik*, 127(5), pp.2653-2658.https://doi.org/10.1016/j.jnoncrysol.2005.11.031

Abdullah, M.M., Suhail, M.H. and Abbas, S.I., 2012. Fabrication and testing of SnO_2 thin films as a gas sensor. *Archives Appl*. Sci. Res, 4(3), pp.1279

Abdullah, N., Ismail, N.M. and Nuruzzaman, D.M., 2018, March. Preparation of tin oxide (SnO_2) thin films using thermal oxidation. In IOP Conference Series*: Materials Science and Engineering* (Vol. 319, p. 012022). IOP Publishing. https://doio.rg10.1088/1757-899X/319/1/012022

AL-Jawad, S.M., Sabr, A.S. and Elttayef, A.K., 2016. Doping effect on structure, optical, & sensing properties of nanocrystalline (SnO_2) thin films prepared by Chemical Bath Deposition (CBD) technique. *Engineering and Technology Journal*, 34(5B), pp.186-197.

Bahade, S.T., Lanje, A.S. and Sharma, S.J., 2017. Synthesis of SnO_2 thin film by sol-gel spin coating technique for optical and ethanol gas sensing application. *International Journal of Scientific Research in Science and Technology* (IJSRST), 3(7), pp.567-575.

Bendjedidi, H., Attaf, A., Saidi, H., Aida, M.S., Semmari, S., Bouhdjar, A. and Benkhetta, Y., 2015. Properties of n-type SnO_2 semiconductor prepared by spray ultrasonic technique for photovoltaic applications. *Journal of Semiconductors, 36(12), p.123002*. https://doi.org/10.1088/1674-4926/36/12/123002

Bendjedidi, H., Attaf, A., Saidi, H., Aida, M.S., Semmari, S., Bouhdjar, A. and Benkhetta, Y., 2015. Properties of n-type SnO_2 semiconductor prepared by spray ultrasonic technique for photovoltaic applications. *Journal of Semiconductors, 36(12), p.123002*. https://doi.org/10.1088/1674-4926/36/12/123002

Benhaoua, B., Abbas, S., Rahal, A., Benhaoua, A. and Aida, M.S., 2015. Effect of film thickness on the structural, optical and electrical properties of SnO_2: F thin films prepared by spray ultrasonic for solar cells applications. *Superlattices and Microstructures, 83, pp.78-88.* https://doi.org/10.1016/j.spmi.2015.03.017

Bhatt, A.S., Ranjitha, R., Santosh, M.S., Ravikumar, C.R., Prashantha, S.C., Maphanga, R.R. and Silva, G.F.L.E., 2020. Optical and electrochemical applications of Li-doped NiO nanostructures synthesized via facile microwave technique. *Materials*, 13(13), p.2961 https://doi.org/10.3390/ma13132961

Bouabdalli, E.M., El Jouad, M., Garmim, T., Touhtouh, S., Louardi, A., Monkade, M. and Hartiti, B., 2021. Preparation and characterization of Nickel and Aluminum-Codoped SnO_2 thin films for optoelectronic applications. *International Journal of Photoenergy*, 2021(1), p.5556441. https://doi.org/10.1155/2021/5556441

Brandenburg, R., 2017. Dielectric barrier discharges: Progress on plasma sources and on the understanding of regimes and single filaments. *Plasma Sources Science and Technology, 26(5), p.053001*https://doi.org/10.1088/1755-1315/1263/1/012050

Bu, T., Gao, H., Yao, Y., Wang, J., Pollard, A.J., Legge, E.J., Clifford, C.A., Delvallée, A., Ducourtieux, S., Lawn, M.A. and Babic, B., 2023. Thickness measurements of graphene oxide flakes using atomic force microscopy: Results of an international interlaboratory comparison. *Nanotechnology, 34(22), p.225702*. https://doi.org/10.1088/1361-6528/acbf58

Chen, X., Du, B., Li, Q. and Liu, J., 2024. Bi2O3 doped indium tin oxide thin films fabricated via liquid metal printing. *Journal of Alloys and Compounds, 976, p.173077.* https://doi.org/10.1016/j.jallcom.2023.173077

Dangi, R., Basnet, B., Pandey, M., Bhusal, S., Budhathoki, B., Parajuli, K., Tiwari, S.K. and Kafle, B.P., 2023. Effect of oxygen vacancy on the crystallinity and optical band gap in tin oxide thin film. *Energies, 16(6), p.2653*. https://doi.org/10.3390/en16062653

Doyan, A., Muliyadi, L., Hakim, S., Munandar, H. and Taufik, M., 2021, February. The effect of dopant material to optical properties: energy band gap Tin Oxide thin film. *In Journal of Physics: Conference*

Series (Vol. 1816, No. 1, p. 012114). IOP Publishing. https://doi.org/10.1088/1742-6596/1816/1/012114

Enoki, H., Nakayama, T. and Echigoya, J., 1992. The Electrical and optical properties of the ZnO-SnO_2 thin films prepared by RF magnetron sputtering. *physica status solidi* (a), 129(1), pp.181-191. https://doi.org/10.1002/pssa.2211290116

Guendouz, H., Bouaine, A. and Brihi, N., 2018. Biphase effect on structural, optical, and electrical properties of Al-Sn codoped ZnO thin films deposited by sol-gel spin-coating technique. *Optik, 158, pp.1342-1348*. https://doi.org/10.1016/j.ijleo.2018.01.025

Gupta, P. and Rathore, V., 2020. A comprehensive review: SnO_2 for photovoltaic and gas sensor applications. *Applied Innovative Research* (AIR), 1(3-4), pp.184-193.

Labreche, F., Berbadj, A., Brihi, N., Karima, R. and Jamoussi, B., 2018. Green photoluminescence, structural and optical properties of Nd-TiO2 thin films. *Optik, 172, pp.63-71*. https://doi.org/10.1016/j.ijleo.2018.06.131

Ma, J., Wang, Y., Ji, F., Yu, X. and Ma, H., 2005. UV–violet photoluminescence emitted from SnO_2: Sb thin films at different temperature. *Materials Letters, 59(17), pp.2142-2145* .https://doi.org/10.1016/j.matlet.2005.02.049

Mazloom, J. and Ghodsi, F.E., 2013. Spectroscopic, microscopic, and electrical characterization of nanostructured SnO_2: Co thin films prepared by sol–gel spin coating technique. *Materials Research Bulletin, 48(4), pp.1468-1476*. https://doi.org/10.1016/j.materresbull.2012.12.069

Mohammed, A.F., 2012. Effect of Post-Oxidation on SnO_2 Thin Films. *Eng. &Tech. Journal, 30(11).*

Mohsin, A.N., Al-Ansari, R.A. and Adil, B.H., 2022, August. Non-thermal plasma effects on of structural and optical properties of Nio: Li thin films prepared by the spray pyrolysis technique. *In AIP Conference Proceedings (Vol. 2437, No. 1). AIP Publishing*. https://doi.org/10.1063/5.0092551

Murbat, H.H., Abdalameer, N.K. and Brrd, A.K., 2018. Effects of non-thermal argon plasma produced at atmospheric pressure on the optical properties of CdO thin films. *Baghdad Science Journal, 15(2), pp.0221-0221*: http://dx.doi.org/10.21123/bsj.2018.15.2.0221

Nasir, Z., Shakir, M., Wahab, R., Shoeb, M., Alam, P., Khan, R.H. and Mobin, M., 2017. Co-precipitation synthesis and characterization of Co doped SnO_2 NPs, HSA interaction via various spectroscopic techniques and their antimicrobial and photocatalytic activities. *International journal of biological macromolecules,* 94, pp.554-565. https://doi.org/10.1016/j.ijbiomac.2016.10.057

Paneru, R., Lamichhane, P., Chandra Adhikari, B., Ki, S.H., Choi, J., Kwon, J.S. and Choi, E.H., 2019. Surface modification of PVA thin film by nonthermal atmospheric pressure plasma for antifogging property. *AIP Advances*, 9(7). https://doi.org/10.1063/1.5100776

Saadeddin, I., Pecquenard, B., Manaud, J.P., Decourt, R., Labrugère, C., Buffeteau, T. and Campet, G., 2007. Synthesis and characterization of single-and co-doped SnO_2 thin films for optoelectronic applications. *Applied Surface Science, 253(12), pp.5240-5249.* https://doi.org/10.1016/j.apsusc.2006.11.049

Sawant, J.P., Pathan, H.M. and Kale, R.B., 2021. Spray pyrolytic deposition of CuInS2 thin films: properties and applications. *Engineered Science*, 13, pp.51-64. https://doi.org/10.30919/es8d1147

Serin, T., Serin, N., Karadeniz, S., Sarı, H., Tuğluoğlu, N. and Pakma, O., 2006. Electrical, structural and optical properties of SnO_2 thin films prepared by spray pyrolysis. *Journal of Non-Crystalline Solids*, 352(3), pp.209-215.

Shi, Y., Hamsen, C., Jia, X., Kim, K.K., Reina, A., Hofmann, M., Hsu, A.L., Zhang, K., Li, H., Juang, Z.Y. and Dresselhaus, M.S., 2010. Synthesis of few-layer hexagonal boron nitride thin film by chemical vapor deposition. *Nano letters, 10(10), pp.4134-4139* https://doi.org/10.1021/nl1023707

Soumya, S.S. and Xavier, T.S., 2022. Effect of cobalt doping on the microstructural, optical and electrical properties of SnO2 thin films by sol-gel spin coating technique. Physica B: *Condensed Matter*, 624, p.413432. https://doi.org/10.1016/j.physb.2021.413432

Vossen, J.L. and Poliniak, E.S., 1972. The properties of very thin RF sputtered transparent conducting films of SnO_2: Sb and In_2O_3: Sn. *Thin Solid Films*, 13(2), pp.281-284. https://doi.org/10.1016/0040-6090(72)90296-9

Xu, L., Li, X. and Yuan, J., 2008. Effect of K-doping on structural and optical properties of ZnO thin films. *Superlattices and Microstructures, 44(3), pp.276-281.* https://doi.org/10.1016/j.spmi.2008.04.004

Yang, J.K., Zhao, H.L., Li, J., Zhao, L.P., Chen, J.J. and Yu, B., 2014. Structural and optical properties and photoluminescence mechanism of fluorine-doped SnO_2 films during the annealing process. *Acta materialia, 62, pp.156-161*. https://doi.org/10.1016/j.actamat.2013.09.043

دراسة تاثير البلازما غير الحرارية على الخواص التركيبية و البصلاية للاغشية الرقيقة المصنوعة من مادة SnO_2: Co بطريقة الرش الحراري

رنده محمد عبدالله *، رامز احمد الانصاري

جامعة بغداد, كلية العلوم للبنات, قسم الفيزياء, بغداد, العراق

الخلاصة

في هذه الدراسة تم استخدام طريقة الرش الحراري لتصنيع اغشية رقيقة من مادة القصدير النقي SnO_2 و كذلك SnO_2: 2%Co و التي تم ترسيبها على قواعد زجاجية مسخنة بدرجة حرارة 400^o حيث تم فحص الخواص التركيبة و البصرية لهذه الاغشية الرقيقة, ثم تم تعريض هذه الاغشية الرقيقة للبلازما بأزمان مختلفة (3,5,7 ثانية) من اجل دراسة تأثير البلازما الباردة على الخواص التركيبية و البصرية لهذه الاغشية, اظهر فحص XRD ان هذه الاغشية SnO_2:Co متعددة التبلور و تملك شكل رباعي, كانت القمم لهذه الاغشية هي (110), (101) و (211) و التي تقابل زاويا الحيود التالية (26.55^o) ,(33.90^o) و (51.55^o), كذلك ظهرت قمة تعود الى Co هذه القمة هي (311) و التي تقابل الزاوية (36.78^o). من خلال فحص ال AFMتوضح ان الحجم الحبيبي قل من 64.01nmالى59.10nm بعد التشويب كذلك لوحظ أيضا ان الخشونة و متوسط مربع الخشونة زادت بعد التشويب، و من خلال فحص ال UV تبين ان النفاذية قد زادت بعد التشويب و قلت بعد تعريضها للبلازما الباردة, بعد تعرض للبلازما الباردة لوحظ ان قيمة فجوة الطاقة و الامتصاصية و الثوابت البصرية جميعها قد زادت قيمتها بعد التعريض للبلازما بفترات زمنية مختلفة (3,5,7 ثانية).

الكلمات المفتاحية: SnO_2:Co, الرش الحراري, البلازما الغير حرارية , الخواص التركيبية , الخواص البصرية